**Geoscientific**
**Model Development**
Discussions

Open Access

# Sensitivity of chemical transport model simulations to the duration of chemical and transport operators: a case study with GEOS-Chem v10-01

**S. Philip[1], R. V. Martin[1,2], and C. A. Keller[3]**

[1]Department of Physics and Atmospheric Science, Dalhousie University, Halifax, Nova Scotia, Canada
[2]Harvard-Smithsonian Center for Astrophysics, Cambridge, MA, USA
[3]School of Engineering and Applied Sciences, Harvard University, Cambridge, MA, USA

Correspondence to: S. Philip (philip.sajeev@dal.ca)

## Abstract

Chemical transport models involve considerable computational expense. Fine temporal resolution offers accuracy at the expense of computation time. Assessment is needed of the sensitivity of simulation accuracy to the duration of chemical and transport op-
5    erators. We conduct a series of simulations with the GEOS-Chem chemical transport model at different temporal and spatial resolutions to examine the sensitivity of simulated atmospheric composition to temporal resolution. Subsequently, we compare the tracers simulated with operator durations from 10 to 60 min as typically used by global chemical transport models, and identify the timesteps that optimize both computational
10   expense and simulation accuracy. We found that longer transport timesteps increase concentrations of emitted species such as nitrogen oxides and carbon monoxide since a more homogeneous distribution reduces loss through chemical reactions and dry deposition. The increased concentrations of ozone precursors increase ozone production at longer transport timesteps. Longer chemical timesteps decrease sulfate and
15   ammonium but increase nitrate due to feedbacks with in-cloud sulfur dioxide oxidation and aerosol thermodynamics. The simulation duration decreases by an order of magnitude from fine (5 min) to coarse (60 min) temporal resolution. We assess the change in simulation accuracy with resolution by comparing the root mean square difference in ground-level concentrations of nitrogen oxides, ozone, carbon monoxide
20   and secondary inorganic aerosols with a finer temporal or spatial resolution taken as truth. Simulation error for these species increases by more than a factor of 5 from the shortest (5 min) to longest (60 min) temporal resolution. Chemical timesteps twice that of the transport timestep offer more simulation accuracy per unit computation. However, simulation error from coarser spatial resolution generally exceeds that from longer
25   timesteps; e.g. degrading from $2° \times 2.5°$ to $4° \times 5°$ increases error by an order of magnitude. We recommend prioritizing fine spatial resolution before considering different temporal resolutions in offline chemical transport models. We encourage the chemical

transport model users to specify in publications the durations of operators due to their effects on simulation accuracy.

# 1 Introduction

Global and regional chemical transport models (CTMs) have a wide range of applications in studies of climate, air quality, and biogeochemical cycling. The last few decades have witnessed rapid development of modeling sophistication to tackle these issues, but that development is associated with increasing computational expense. Eulerian models divide the atmosphere into numerous ($10^4$–$10^8$) grid boxes and solve a mass continuity equation to simulate atmospheric composition. The concentrations of the simulated species are sensitive to the temporal resolution of the CTM. Attention is needed to understand how temporal resolution affects model performance.

Numerous studies have examined the sensitivity of simulations to grid resolution for ozone (Jang et al., 1995a, b; Esler et al., 2004; Wild and Prather, 2006), ozone production efficiency (Liang and Jacobson, 2000), and ozone sensitivity to precursor emissions (Cohan et al., 2006). Biases can be reduced by simulating sub grid scale processes such as emission plumes from point sources (Sillman et al., 1990; Gillani and Pleim, 1996), aircraft exhaust (Meijer et al., 1997; Kraabol et al., 2002), ship exhaust (Vinken et al., 2011), and lightning (Cooper et al., 2014). Simulation error increases proportional to the size of the horizontal grid (Wild and Prather, 2006; Prather et al., 2008). The spatiotemporal variation of tropospheric carbon monoxide is better represented with finer grid resolution (Wang et al., 2004; Chen et al., 2009; Yan et al., 2014). Moreover, fine horizontal resolution is important for air quality exposure assessment and health impact studies (Punger and West, 2013; Fountoukis et al., 2013; Thompson et al., 2014; Li et al., 2015). Fine vertical resolution can better represent convection (Rind et al., 2007; Arteta et al., 2009). Simulations are also sensitive to temporal resolution (Mallet et al., 2007; Mallet and Sportisse, 2006), however, few studies have examined this sensitivity.

CTMs solve the continuity equation of around hundred chemical species, each with number density $n$, for individual grid boxes defined in the Eulerian model.

$$\frac{\partial n}{\partial t} = -\nabla \cdot nU + P - L \tag{1}$$

$\partial n/\partial t$ represents the local temporal evolution of $n$. $-\nabla \cdot nU$ represents the transport flux divergence term, where $U$ is the wind velocity vector. $P$ and $L$ are the local production and loss terms respectively. Typically, the above equation is discretized in space, and the continuity equation is simulated as a system of coupled non-linear partial differential equations with chemical and transport operators. These operators are usually simulated sequently through operator splitting (McRae et al., 1982) which is found to increase computational efficiency (Kim and Cho, 1997). The transport operator involves solving the 3-D advection equation using efficient numerical schemes (Prather, 1986; Rood, 1987). The Courant number $C_r$ which relates the product of the wind speed $u$ and the transport timestep $T$ to the length of the grid box $x$,

$$C_r = \frac{u \times T}{x} \tag{2}$$

is kept less than unity for stability in advection schemes based on the Courant–Freidrich–Lewy criterion (Courant et al., 1967). Semi-Lagrangian numerical schemes (Lin and Rood, 1996) have been developed to accommodate higher $C_r$, and thereby allow coarser transport timesteps for faster computation. The chemical operator representing the temporal evolution of local sources and sinks involves numerically solving a system of coupled ordinary differential equations using efficient solvers (Hertel et al., 1993; Jacobson and Turco, 1994; Damian et al., 2002). For computational convenience, production and loss terms are also simulated as individual operators. The order in which operators are applied can affect performance (Sportisse, 2000; Santillana et al., 2015). The operator splitting method requires the coupling between individual operators to be negligible over each timestep. However, reducing timesteps increases computational expense. Attention is needed to this tradeoff.

Full Screen / Esc

Printer-friendly Version

Interactive Discussion

We examine the sensitivity of a CTM to temporal resolution by conducting a series of simulations at different temporal and horizontal resolutions. We then identify the optimal temporal resolution for the range of timesteps from 10 to 60 min as usually used by global CTMs (e.g., Horowitz et al., 2003; Huijnen et al., 2010). Section 2 describes the sensitivity simulations, as well as the method to quantify the simulation error, and the method to identify the simulation timesteps that best account for both computational expense and simulation accuracy. Comparison of the sensitivity simulations, description of resolution-dependent errors, and the identification of appropriate chemical and transport timesteps are examined in Sect. 3.

## 2 Materials and methods

### 2.1 GEOS-Chem simulations

We conduct a series of sensitivity simulations with the GEOS-Chem CTM (version 10-01; www.geos-chem.org) at different temporal and horizontal resolutions to examine the individual sensitivities to chemical and transport timestep durations. The GEOS-Chem model (Bey et al., 2001) is used by about 100 research groups worldwide to simulate the oxidant-aerosol system. GEOS-Chem has the capability to be driven with several generations of assimilated meteorological data from the Goddard Earth Observing System (GEOS) at the NASA Global Modeling Assimilation Office (GMAO). For computational expedience, GEOS-Chem global simulations are often conducted using horizontal resolutions of either $4° × 5°$ or $2° × 2.5°$ degraded from the native resolution of GEOS meteorology. GEOS-Chem also has the capability for nested regional simulations where the global model provides dynamic boundary condition to the regional grids (Wang et al., 2004; Chen et al., 2009; Zhang et al., 2011; van Donkelaar et al., 2012). We use the GEOS-5 (or GEOS-5.2.0) meteorology available at a native horizontal resolution of $0.5° × 0.667°$ (Rienecker et al., 2008). It includes three-hour averaged 2-D fields like mixed layer depth, and six-hour averaged 3-D fields such as

zonal and meridional wind, convective mass flux. The height of the lowest level of the model is approximately 130 m above the sea level, with 47 vertical levels.

GEOS-Chem performs tracer advection ($A$), vertical mixing ($V$), cloud convection ($Z$) and wet deposition ($W$) for every transport timestep ($T$), as well as dry deposition ($D$), emissions ($E$), and chemistry ($G$) for every chemical timestep ($C$) in the following order,

$$A(T) \times D(C) \times E(C) \times V(T) \times Z(T) \times G(C) \times W(T) \tag{3}$$

The traditional transport timesteps are 30 min for the 4° × 5° resolution, 15 min for the 2° × 2.5° resolution, 10 min for 0.5° × 0.667° resolution, and 5 min for 0.25° × 0.312° simulations. The traditional chemical timesteps have varied from either 60 min or twice the transport timestep based on the Strang operator splitting scheme (Strang, 1968) which follows $T \times C \times T \times T \times C \times T$ order repetitively with $C = 2 \times T$. We also test an alternate splitting scheme which follows $T \times C \times T \times C$ order repetitively with $C = T$.

Advection is based on the multi-dimensional flux-form semi-Lagrangian advection scheme (Lin and Rood, 1996; Lin et al., 1994), with an additional pressure-fixer algorithm implemented for the conservation of tracer mass (Rotman et al., 2004). Transport by convection is coupled (Balkanski et al., 1993; Wu et al., 2007) with gas-aerosol wet deposition (Liu et al., 2001; Wang et al., 2011; Amos et al., 2012). GEOS-Chem uses an internal timestep of 5 min for convective mixing. We use a non-local boundary layer mixing scheme for vertical transport (Holtslag and Boville, 1993; Lin and McElroy, 2010).

Emissions are processed through the HEMCO module (Keller et al., 2014). A resistance-in-series method is used for dry deposition of species (Wesely, 1989; Wang et al., 1998; Zhang et al., 2001; Fisher et al., 2011).

GEOS-Chem uses a Sparse Matrix Vectorized GEAR II chemistry solver (Jacobson and Turco, 1994; Jacobson, 1995, 1998). The oxidant-aerosol chemistry simulation includes organic and black carbon (Park et al., 2003), mineral dust (Fairlie et al., 2007), sea salt (Alexander et al., 2005; Jaegle et al., 2011), and the sulfate-nitrate-ammonium system (Park et al., 2004). The photolysis frequency is calculated (Mao et al., 2010)

at the middle of the chemical timestep using the Fast-JX algorithm (Bian and Prather, 2002). Simulation of gas-aerosol interactions are performed by aerosol extinction effects on photolysis rates (Martin et al., 2003), and heterogeneous chemistry (Jacob, 2000) with aerosol uptake of $N_2O_5$ (Evans and Jacob, 2005) and $HO_2$ (Mao et al., 2013). The ISORROPIA II thermodynamic module (Fontoukis and Nenes, 2007) performs aerosol-gas partitioning (Pye et al., 2009).

We conduct simulations for 2010 July at two horizontal resolutions of $4° × 5°$ and $2° × 2.5°$ globally, and $0.5° × 0.667°$ over the North America (140–40° W, 10–70° N) and East Asia (70–150° W, 11° S–55° N) nested regions. We use the $4° × 5°$ global simulation to archive dynamic boundary conditions every three hours for the nested models. We use one month spin up with each GEOS-Chem simulation to reduce the influence of initial conditions.

## 2.2 Computing platform

We conduct all simulations on the same computing platform to compare their computational performance. We use the Glooscap cluster of the Atlantic Computational Excellence Network (ACENET) Consortium of Canadian Universities (http://www.ace-net.ca/wiki/Glooscap). The operating system is Linux 4.8. We use Intel Fortran compiler version 12. Each GEOS-Chem simulation is submitted as a 16-thread parallelized job on a single node.

We calculate the CPU time for the month of July for each operator separately using the Fortran-intrinsic routine, CPU_TIME. We found this value identical to the one calculated using the Linux command "qacct –j". To reduce the effects of other jobs on the shared cluster, we repeat simulations five times, while excluding data output operations to minimize sensitivity to system input/output, and use the median to represent CPU time.

## 2.3 Assessing simulation error

Assessing simulation error vs. timestep through comparison with observations is impaired by imperfect model processes, by the sparseness of measurements, and by model-observation representativeness biases. Therefore, we treat the simulation with the finest temporal resolution as the most accurate. We take as "Truth" the concentrations simulated with a chemical timestep ($C$) of 10 min and a transport time step ($T$) of 5 min (represented as C10T05). Finer resolutions are computationally prohibitive. We define the simulation error $E_{sim}^s$ for species $s$ as the root mean square error (RMSE) of the species concentrations simulated with the finest resolution (Truth) and the simulation under consideration (Sim), normalized by the concentrations in simulation "Truth",

$$E_{sim}^s = \frac{\sqrt{\sum_{i=1}^{i=N} (\text{Truth}_i^s - \text{Sim}_i^s)^2}}{\sum_{i=1}^{i=N} \text{Truth}_i^s} \tag{4}$$

where, $i$ represents a particular grid box, with a total number of $N$ grid boxes of interest. RMSE in the numerator is chosen instead of absolute difference to more heavily penalize extrema. Normalization with the mass of the true simulation is intended to cross-compare $E_{sim}^s$ of different species. $E_{sim}^s$ captures the variation of a species $s$ from the true simulation.

Here, we focus on four key species relevant to atmospheric chemistry, namely nitrogen oxides ($NO_x = NO + NO_2$), ozone ($O_3$), carbon monoxide (CO), and secondary inorganic aerosols (SIA: sum of sulfate, nitrate and ammonium). These species represent a range of lifetimes from a day ($NO_x$) to weeks (CO). The focus on SIA is designed to devote more attention to chemically active species than to mineral dust and sea salt. We sample the instantaneous values of simulated ground-level concentrations of these atmospheric species every 60 min to span the diurnal variation of chemical environ-

ments. We focus on concentrations in July near the Earth's surface when and where chemical and transport timescales tend to be short.

## 2.4 Identifying the optimal temporal resolution

A practical way to select optimal chemical and transport timesteps is to identify the
simulation with the lowest error ($E_{sim}^s$) per unit of computation time. To quantify the simulation accuracy per unit CPU time, we propose a simple metric, the normalized error (NE) which represents a tradeoff between the simulation accuracy, and the associated computation expense. This is performed by normalizing the simulation error $E_{sim}^s$ for species $s$ by the CPU time $t$ for the simulation under consideration $t_{sim}$ and for
a reference simulation $t_{ref}$, and taking the mean of four species.

$$NE = \left( \frac{1}{4} \times \sum_s \frac{E_{sim}^s}{E_{ref}^s} \right) \times \left( \frac{t_{sim}}{t_{ref}} \right) \tag{5}$$

We normalize $E_{sim}^s$ by the reference $E_{ref}^s$ so that the normalized error for each species is of similar magnitude. The variation of NE across timesteps is unaffected by the choice of reference simulation; C10T10 is used here. The simulation with the lowest NE can
identify an optimal chemical and transport resolution.


## 3 Results and discussion

Figure 1 shows the computational performance for the series of GEOS-Chem simulations conducted here. The CPU time decreases by an order of magnitude from fine to coarse temporal resolution. The CPU time increases by about a factor of 4 from
4° × 5° to 2° × 2.5° and another factor of 2 to a single nested simulation at 0.5° × 0.667°. Comparison of individual CPU times for chemical and transport operators shows that performing a single cycle of all chemical operations takes ∼ 4 times that of a single
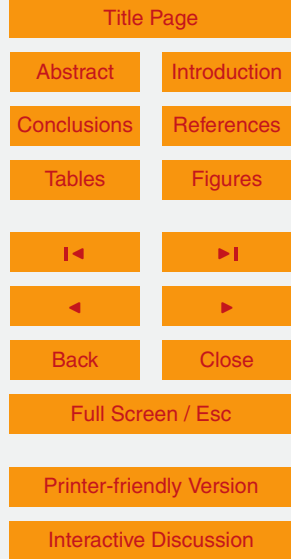
cycle of transport operations at the global scale. This factor is reduced for nested simulations due in part to the additional CPU time for simulating boundary conditions.

Figure 2 illustrates the sensitivity of the simulations to chemical and transport operators at $2° \times 2.5°$ horizontal resolution. The left columns show the tracer concentrations for the "true" simulation (C10T05). The middle column shows the difference in tracer concentrations from doubling the transport timestep duration. Increasing the transport timestep tends to increase concentrations of emitted species like CO and $NO_x$ over source regions since tracers are more uniformly mixed by long timesteps before loss processes such as deposition and chemistry occur. More homogeneous fields have lower dry deposition and chemical loss rates. The increase in CO decreases OH over source regions. Increasing concentrations of ozone precursors increases ozone production ($P[O_3]$). Wild and Prather (2006) similarly found that ozone production increases at coarser horizontal resolution. Increasing the transport timestep duration increases SIA components, especially over the source regions of East Asia, North India, and North America.

The right column in Fig. 2 shows the change in tracer concentrations from increasing the chemical timestep. Hydroxyl radical concentrations increase, $NO_x$ concentrations decrease, and $P[O_3]$ decreases with increasing chemical timesteps over source regions. Berntsen and Isaken (1997) found that the error introduced by coarser chemical timesteps is higher in polluted regions than the clean background due to the increased time lag, and invariant production and loss across rapid chemical cycles. A longer chemical timestep decreases sulfate and ammonium but increases nitrate over source regions. Inspection of $SO_2$ and $H_2O_2$ fields indicates that sulfate formation through $H_2O_2$ in clouds decreases at longer chemical timesteps. In turn, $SO_2$ and $NH_3$ concentrations increase at longer chemical timesteps due to the corresponding decreases in ammonium sulfate or ammonium bisulfate. The additional free ammonia at longer chemical timesteps tends to promote regional ammonium nitrate formation depending on local thermodynamics. An increase of total SIA mass with the increasing chemical timestep is driven by nitrate and ammonium, and partially compensated by a reduction

in sulfate, especially downwind of source regions. We found similar spatial patterns for other timestep combinations, and other horizontal resolutions.

Figure 3 shows the simulation error for nitrogen oxides, ozone, carbon monoxide and secondary inorganic aerosols with varying temporal resolution at $2° \times 2.5°$ horizontal resolution. Simulation errors for all these major species increase by more than a factor of 5 from the shortest to longest temporal resolution. Errors increase fairly smoothly with increasing chemical and transport timestep until the transport timestep exceeds 30 min. Then the large Courant number increases errors by an order of magnitude for long lived species of $O_3$ and CO. Simulation errors for other horizontal resolutions follows similar pattern.

Figure 4 shows the difference in simulated tracers at $2° \times 2.5°$ horizontal resolution for the GEOS-Chem traditional (C30T15) minus the finest timesteps considered (C10T05). The spatial variation for the monthly mean ground-level concentrations is generally within 5–15 % for short lived species like $NO_x$ and SIA, and within 1 % for longer lived species like $O_3$ and CO. Santillana et al. (2015) similarly found an upper limit of 10 % for operator splitting errors. However, the maximum hourly spatial variation can exceed 50 % for short lived species and 5 % for the longer lived species. The spatial pattern of extrema resembles that of the monthly mean, albeit with more heterogeneity from synoptic variation.

We also examined the diurnal variation and vertical profile of extrema. Extrema arise from all times of day with a slight tendency for larger values for $NO_x$ at night, for ozone near sunrise and sunset, and for SIA and CO near noon. Zonal mean vertical profiles exhibit largest differences in the lower troposphere for $NO_x$ and SIA, with more homogeneous differences throughout the troposphere for $O_3$ and CO. Near the subtropical jets of the upper troposphere $O_3$ and CO have maximum extrema of up to 3 %.

Figure 5 shows the normalized error for the GEOS-Chem simulations at various spatial and temporal resolutions. The NE is significantly higher with $C = T$ than $C = 2 \times T$. We confirmed this tendency with different choices of truth (such as C05T05, C10T10) or reference (such as C10T05) simulations. This finding motivates the traditional ap-

Full Screen / Esc

Printer-friendly Version

Interactive Discussion

proach of using $C = 2 \times T$ in prior GEOS-Chem simulations. Applying the chemical operator as frequently as the transport operator (with $C = T$) appears to increase computation cost with little benefit in accuracy. The NE for all three horizontal resolutions has a noisy minima with a chemical timestep of 20 min and a transport timestep of 10 min (C20T10). A unit of computation time has a similar efficiency for a small range of timesteps from 10 to 20 min. We found similar patterns in the variation of NE with timesteps with NE calculated for selected domains, such as over Northern Hemisphere, nested model regions, land grid boxes, and over the entire troposphere. We conducted additional simulations at $4° \times 5°$ horizontal resolution for January 2011 with a spin up of 7 months, and found similar patterns in NE.

The simulation error decreases by 40–50 % (Fig. 3) by changing the resolution from the traditional (C30T15) to the optimal (C20T10) at $2° \times 2.5°$ horizontal resolution. The relative spatial variations are < 10 % for $NO_x$ and SIA, and < 1 % for $O_3$ and CO. However, the CPU time increases by 20 % by the increase in temporal resolution.

Table 1 shows the simulation error at $4° \times 5°$ horizontal resolution with truth at $2° \times 2.5°$ resolution (C10T05) to investigate the tradeoff between temporal and horizontal resolution. The simulation error for all species at $4° \times 5°$ resolution increases by an order of magnitude compared to $2° \times 2.5°$ resolution for any choice of timestep tested here. The error in this configuration is dominated by representativeness differences between $4° \times 5°$ and is insensitive to timestep. Numerical errors due to advection processes generally exceed those from operator splitting (e.g., Prather et al., 2008; Santillana et al., 2015). We therefore recommend prioritizing horizontal resolution over temporal resolution for offline CTMs using time-averaged meteorological fields as tested here. As meteorological fields used in CTMs become available at finer temporal resolution, the value of shorter timesteps should further increase. We encourage the CTM users to specify the durations of operators in publications due to its effect on simulation accuracy.

**Sensitivity of CTM simulations to the temporal resolution**

S. Philip et al.

Title Page

Abstract  Introduction

Conclusions  References

Tables  Figures

◄  ►

◄  ►

Back  Close

Full Screen / Esc

Printer-friendly Version

Interactive Discussion

## 4   Conclusions

The computational expense of chemical transport models warrants investigation into their efficiency and accuracy. Solving the continuity equation in CTMs through operator splitting method offers numerical efficiency, however, few studies have examined the implications of operator duration on simulation accuracy. We conducted simulations with the GEOS-Chem model for multiple choices of timestep duration from 10 to 60 min as typically used by global CTMs. We found that longer transport timesteps increase ozone precursors and ozone production over source regions since a more homogeneous distribution reduces loss through chemical reactions and dry deposition. Longer chemical timesteps decrease $NO_x$ and ozone production over source regions. Longer chemical timesteps reduce sulfate and ammonium concentrations, however increase nitrate due to feedbacks with in-cloud $SO_2$ oxidation and local aerosol thermodynamics.

We investigated the computational efficiency with the GEOS-Chem model, and found that the simulation duration decreases by an order of magnitude from fine (C10T05) to coarse (C60T60) temporal resolution. The chemical operator consumes about four times the CPU time of the transport operator. We subsequently compared the root mean square differences in the ground-level concentrations of nitrogen oxides, ozone, carbon monoxide and secondary inorganic aerosols with a finer temporal or spatial resolution taken as truth, and estimated the simulation error. Simulation error for these species increases by more than a factor of 5 from the shortest to longest temporal resolution.

In order to account for simulation accuracy with computational cost, we proposed a metric, normalized error that identifies the temporal resolution with respect to CPU cost. We recommend the approach of using $C = 2 \times T$ for all horizontal resolutions. The normalized error exhibits a noisy minimum for a chemical timestep of 20 min and transport timestep of 10 min for the horizontal and temporal resolutions considered here. Nonetheless, the simulation error from changing spatial resolution exceeds that from changing temporal resolution. We recommend choosing the finest possible spa-

tial resolution before considering different temporal resolutions in offline CTMs with time-averaged archived meteorological fields as tested here. The importance of shorter timesteps should increase with the availability of time-averaged meteorological fields at higher temporal resolution. Short operator timesteps could offer even greater bene-
5  fits to simulation accuracy in online CTMs that offer meteorological fields at temporal resolutions closer to timestep duration. We encourage the CTM users to specify in publications the durations of operators due to their effects on simulation accuracy.

## Code availability

The GEOS-Chem code is freely accessible to the public, by following the guidelines in
10  http://wiki.geos-chem.org/). This work used GEOS-Chem version 10-01.

## References

Alexander, B., Park, R. J., Jacob, D. J., Li, Q. B., Yantosca, R. M., Savarino, J., Lee, C. C. W., and
15     Thiemens, M. H.: Sulfate formation in sea-salt aerosols: constraints from oxygen isotopes, J. Geophys. Res., 110, D10307, doi:10.1029/2004JD005659, 2005.
Amos, H. M., Jacob, D. J., Holmes, C. D., Fisher, J. A., Wang, Q., Yantosca, R. M., Corbitt, E. S., Galarneau, E., Rutter, A. P, Gustin, M. S., Steffen, A., Schauer, J. J., Graydon, J. A., Louis, V. L. St., Talbot, R. W., Edgerton, E. S., Zhang, Y., and Sunderland, E. M.:
20     Gas-particle partitioning of atmospheric Hg(II) and its effect on global mercury deposition, Atmos. Chem. Phys., 12, 591–603, doi:10.5194/acp-12-591-2012, 2012.
Arteta, J., Marécal, V., and Rivière, E. D.: Regional modelling of tracer transport by tropical convection – Part 2: Sensitivity to model resolutions, Atmos. Chem. Phys., 9, 7101–7114, doi:10.5194/acp-9-7101-2009, 2009.
25  Balkanski, Y. J., Jacob, D. J., Gardner, G. M., Graustein, W. C., and Turekian, K. K.: Transport and residence times of tropospheric aerosols inferred from a global three-dimensional simulation of 210Pb, J. Geophys. Res., 98, 20573–20586, doi:10.1029/93JD02456, 1993.

Berntsen, T. K. and Isaksen, I. S. A.: A global three-dimensional chemical transport model for the troposphere: 1. Model description and CO and ozone results, J. Geophys. Res., 102, 21239–21280, doi:10.1029/97JD01140, 1997.

Bey, I., Jacob, D. J., Yantosca, R. M., Logan, J. A., Field, B. D., Fiore, A. M., Li, Q. B., Liu, H. G. Y., Mickley, L. J., and Schultz, M. G.: Global modeling of tropospheric chemistry with assimilated meteorology: model description and evaluation, J. Geophys. Res., 106, 23073–23095, doi:10.1029/2001JD000807, 2001.

Bian, H. and Prather, M. J.: Fast-J2: Accurate simulation of stratospheric photolysis in global chemical models, J. Atmos. Chem., 41, 281–296, doi:10.1023/A:1014980619462, 2002.

Chen, D., Wang, Y., McElroy, M. B., He, K., Yantosca, R. M., and Le Sager, P.: Regional CO pollution and export in China simulated by the high-resolution nested-grid GEOS-Chem model, Atmos. Chem. Phys., 9, 3825–3839, doi:10.5194/acp-9-3825-2009, 2009.

Cohan, D. S., Hu, Y., and Russell, A. G.: Dependence of ozone sensitivity analysis on grid resolution, Atmos. Environ., 40, 126–135, doi:10.1016/j.atmosenv.2005.09.031, 2006.

Cooper, M., Martin, R. V., Wespes, C., Coheur, P., Clerbaux, C., and Murray, L. T.: Tropospheric nitric acid columns from the IASI satellite instrument interpreted with a chemical transport model: implications for parameterizations of nitric oxide production by lightning, J. Geophys. Res.-Atmos., 119, 10068–10079, doi:10.1002/2014JD021907, 2014.

Courant, R., Friedrichs, K., and Lewy, H.: On partial difference equations of mathematical physics, IBM J. Res. Dev., 11, 215–234, doi:10.1147/rd.112.0215, 1967.

Damian, V., Sandu, A., Damian, M., Potra, F., and Carmichael, G. R.: The kinetic preprocessor KPP-a software environment for solving chemical kinetics, Comput. Chem. Eng., 26, 1567–1579, doi:10.1016/S0098-1354(02)00128-X, 2002.

Esler, J. G., Roelofs, G. J., Köhler, M. O., and O'Connor, F. M.: A quantitative analysis of grid-related systematic errors in oxidising capacity and ozone production rates in chemistry transport models, Atmos. Chem. Phys., 4, 1781–1795, doi:10.5194/acp-4-1781-2004, 2004.

Evans, M. J. and Jacob, D. J.: Impact of new laboratory studies of $N_2O_5$ hydrolysis on global model budgets of tropospheric nitrogen oxides, ozone, and OH, Geophys. Res. Lett., 32, L09813, doi:10.1029/2005GL022469, 2005.

Fairlie, T. D., Jacob, D. J., and Park, R. J.: The impact of transpacific transport of mineral dust in the United States, Atmos. Environ., 41, 1251–1266, doi:10.1016/j.atmosenv.2006.09.048, 2007.

Title Page

Abstract | Introduction

Conclusions | References

Tables | Figures

◀ | ▶|

◀ | ▶

Back | Close

Full Screen / Esc

Printer-friendly Version

Interactive Discussion

Fisher, J. A., Jacob, D. J., Wang, Q., Bahreini, R., Carouge, C. C., Cubison, M. J., Dibb, J. E., Diehl, T., Jimenez, J. L., Leibensperger, E. M., Lu, Z., Meinders, M. B. J., Pye, H. O. T., Quinn, P. K., Sharma, S., Streets, D. G., van Donkelaar, A., and Yantosca, R. M.: Sources, distribution, and acidity of sulfate-ammonium aerosol in the Arctic in winter-spring, Atmos. Environ., 45, 7301–7318, doi:10.1016/j.atmosenv.2011.08.030, 2011.

Fountoukis, C. and Nenes, A.: ISORROPIA II: a computationally efficient thermodynamic equilibrium model for $K^+$–$Ca^{2+}$–$Mg^{2+}$–$NH_4^+$–$Na^+$–$SO_4^{2-}$–$NO_3^-$–$Cl^-$–$H_2O$ aerosols, Atmos. Chem. Phys., 7, 4639–4659, doi:10.5194/acp-7-4639-2007, 2007.

Fountoukis, C., Koraj, D., Denier van der Gon, H. A. C., Charalampidis, P. E., Pilinis, C., and Pandis, S. N.: Impact of grid resolution on the predicted fine PM by a regional 3-D chemical transport model, Atmos. Environ., 68, 24–32, doi:10.1016/j.atmosenv.2012.11.008, 2013.

Gillani, N. V. and Pleim, J. E.: Sub-grid-scale features of anthropogenic emissions of $NO_x$ and VOC in the context of regional Eulerian models, Atmos. Environ., 30, 2043–2059, doi:10.1016/1352-2310(95)00201-4, 1996.

Hertel, O., Berkowicz, R., Christensen, J., and Hov, Ø.: Test of two numerical schemes for use in atmospheric transport-chemistry models, Atmos. Environ. A-Gen., 27, 2591–2611, doi:10.1016/0960-1686(93)90032-T, 1993.

Holtslag, A. A. M. and Boville, B. A.: Local versus nonlocal boundary-layer diffusion in a global climate model, J. Climate, 6, 1825–1842, doi:10.1175/1520-0442(1993)006<1825:LVNBLD>2.0.CO;2, 1993.

Horowitz, L. W., Walters, S., Mauzerall, D. L., Emmons, L. K., Rasch, P. J., Granier, C., Tie, X., Lamarque, J., Schultz, M. G., Tyndall, G. S., Orlando, J. J., and Brasseur, G. P.: A global simulation of tropospheric ozone and related tracers: description and evaluation of MOZART, version 2, J. Geophys. Res., 108, 4784, doi:10.1029/2002JD002853, 2003.

Huijnen, V., Williams, J., van Weele, M., van Noije, T., Krol, M., Dentener, F., Segers, A., Houweling, S., Peters, W., de Laat, J., Boersma, F., Bergamaschi, P., van Velthoven, P., Le Sager, P., Eskes, H., Alkemade, F., Scheele, R., Nédélec, P., and Pätz, H.-W.: The global chemistry transport model TM5: description and evaluation of the tropospheric chemistry version 3.0, Geosci. Model Dev., 3, 445–473, doi:10.5194/gmd-3-445-2010, 2010.

Jacob, D.: Heterogeneous chemistry and tropospheric ozone, Atmos. Environ., 34, 2131–2159, doi:10.1016/S1352-2310(99)00462-8, 2000.

Jacobson, M. Z.: Computation of global photochemistry with SMVGEAR II, Atmos. Environ., 29, 2541–2546, doi:10.1016/1352-2310(95)00194-4, 1995.

Jacobson, M. Z.: Improvement of SMVGEAR II on vector and scalar machines through absolute error tolerance control, Atmos. Environ., 32, 791–796, doi:10.1016/S1352-2310(97)00315-4, 1998.

Jacobson, M. and Turco, R. P.: SMVGEAR – a sparse-matrix, vectorized gear code for atmospheric models, Atmos. Environ., 28, 273–284, doi:10.1016/1352-2310(94)90102-3, 1994.

Jaeglé, L., Quinn, P. K., Bates, T. S., Alexander, B., and Lin, J.-T.: Global distribution of sea salt aerosols: new constraints from in situ and remote sensing observations, Atmos. Chem. Phys., 11, 3137–3157, doi:10.5194/acp-11-3137-2011, 2011.

Jang, J. C., Jeffries, H. E., Byun, D., and Pleim, J. E.: Sensitivity of ozone to model grid resolution – I. Application of high-resolution regional acid deposition model, Atmos. Environ., 29, 3085–3100, doi:10.1016/1352-2310(95)00118-I, 1995b.

Jang, J. C., Jeffries, H. E., and Tonnesen, S.: Sensitivity of ozone to model grid resolution – II. Detailed process analysis for ozone chemistry, Atmos. Environ., 29, 3101–3114, doi:10.1016/1352-2310(95)00119-J, 1995a.

Keller, C. A., Long, M. S., Yantosca, R. M., Da Silva, A. M., Pawson, S., and Jacob, D. J.: HEMCO v1.0: a versatile, ESMF-compliant component for calculating emissions in atmospheric models, Geosci. Model Dev., 7, 1409–1417, doi:10.5194/gmd-7-1409-2014, 2014.

Kim, J. and Cho, S. Y.: Computation accuracy and efficiency of the time-splitting method in solving atmospheric transport/chemistry equations, Atmos. Environ., 31, 2215–2224, doi:10.1016/S1352-2310(97)88636-0, 1997.

Kraabøl, A. G., Berntsen, T. K., Sundet, J. K., and Stordal, F.: Impacts of $NO_x$ emissions from subsonic aircraft in a global three-dimensional chemistry transport model including plume processes, J. Geophys. Res., 107, 4655, doi:10.1029/2001JD001019, 2002.

Li, Y., Henze, D. K., Jack, D., and Kinney, P.: The influence of air quality model resolution on health impact assessment for fine particulate matter and its components, Air Qual. Atmos. Health, 1–18, doi:10.1007/s11869-015-0321-z, 2015.

Liang, J. and Jacobson, M. Z.: Effects of subgrid segregation on ozone production efficiency in a chemical model, Atmos. Environ., 34, 2975–2982, doi:10.1016/S1352-2310(99)00520-8, 2000.

Lin, J. and McElroy, M. B.: Impacts of boundary layer mixing on pollutant vertical profiles in the lower troposphere: implications to satellite remote sensing, Atmos. Environ., 44, 1726–1739, doi:10.1016/j.atmosenv.2010.02.009, 2010.

Lin, S. and Rood, R. B.: Multidimensional flux-form semi-Lagrangian transport schemes, Mon. Weather Rev., 124, 2046–2070, doi:10.1175/1520-0493(1996)124<2046:MFFSLT>2.0.CO;2, 1996.

Lin, S., Chao, W. C., Sud, Y. C., and Walker, G. K.: A class of the van Leer-type transport schemes and its application to the moisture transport in a general circulation model, Mon. Weather Rev., 122, 1575–1593, doi:10.1175/1520-0493(1994)122<1575:ACOTVL>2.0.CO;2, 1994.

Liu, H. Y., Jacob, D. J., Bey, I., and Yantosca, R. M.: Constraints from Pb-210 and Be-7 on wet deposition and transport in a global three-dimensional chemical tracer model driven by assimilated meteorological fields, J. Geophys. Res.-Atmos., 106, 12109–12128, doi:10.1029/2000JD900839, 2001.

Mallet, V. and Sportisse, B.: Uncertainty in a chemistry-transport model due to physical parameterizations and numerical approximations: an ensemble approach applied to ozone modeling, J. Geophys. Res., 111, D01302, doi:10.1029/2005JD006149, 2006.

Mallet, V., Pourchet, A., Quélo, D., and Sportisse, B.: Investigation of some numerical issues in a chemistry-transport model: gas-phase simulations, J. Geophys. Res., 112, D15301, doi:10.1029/2006JD008373, 2007.

Mao, J., Jacob, D. J., Evans, M. J., Olson, J. R., Ren, X., Brune, W. H., Clair, J. M. St., Crounse, J. D., Spencer, K. M., Beaver, M. R., Wennberg, P. O., Cubison, M. J., Jimenez, J. L., Fried, A., Weibring, P., Walega, J. G., Hall, S. R., Weinheimer, A. J., Cohen, R. C., Chen, G., Crawford, J. H., McNaughton, C., Clarke, A. D., Jaeglé, L., Fisher, J. A., Yantosca, R. M., Le Sager, P., and Carouge, C.: Chemistry of hydrogen oxide radicals ($HO_x$) in the Arctic troposphere in spring, Atmos. Chem. Phys., 10, 5823–5838, doi:10.5194/acp-10-5823-2010, 2010.

Mao, J., Fan, S., Jacob, D. J., and Travis, K. R.: Radical loss in the atmosphere from Cu-Fe redox coupling in aerosols, Atmos. Chem. Phys., 13, 509–519, doi:10.5194/acp-13-509-2013, 2013.

Martin, R. V., Jacob, D. J., Yantosca, R. M., Chin, M., and Ginoux, P.: Global and regional decreases in tropospheric oxidants from photochemical effects of aerosols, J. Geophys. Res., 108, 4097, doi:10.1029/2002JD002622, 2003.

McRae, G. J., Goodin, W. R., and Seinfeld, J. H.: Numerical solution of the atmospheric diffusion equation for chemically reacting flows, J. Comput. Phys., 45, 1–42, doi:10.1016/0021-9991(82)90101-2, 1982.

Title Page

Abstract | Introduction

Conclusions | References

Tables | Figures

◄ | ►►

◄ | ►

Back | Close

Full Screen / Esc

Printer-friendly Version

Interactive Discussion

Meijer, E. W., van Velthoven, P. F. J., Wauben, W. M. F., Beck, J. P., and Velders, G. J. M.: The effects of the conversion of nitrogen oxides in aircraft exhaust plumes in global models, Geophys. Res. Lett., 24, 3013–3016, doi:10.1029/97GL53156, 1997.

Park, R. J., Jacob, D. J., Chin, M., and Martin, R. V.: Sources of carbonaceous aerosols over the United States and implications for natural visibility, J. Geophys. Res.-Atmos., 108, 4355, doi:10.1029/2002JD003190, 2003.

Park, R. J., Jacob, D. J., Field, B. D., Yantosca, R. M., and Chin, M.: Natural and transboundary pollution influences on sulfate-nitrate-ammonium aerosols in the United States: implications for policy, J. Geophys. Res.-Atmos., 109, D15204, doi:10.1029/2003JD004473, 2004.

Prather, M. J.: Numerical advection by conservation of second-order moments, J. Geophys. Res., 91, 6671–6681, doi:10.1029/JD091iD06p06671, 1986.

Prather, M. J., Zhu, X., Strahan, S. E., Steenrod, S. D., and Rodriguez, J. M.: Quantifying errors in trace species transport modeling, P. Natl. Acad. Sci. USA, 105, 19617–19621, doi:10.1073/pnas.0806541106, 2008.

Punger, E. M. and West, J. J.: The effect of grid resolution on estimates of the burden of ozone and fine particulate matter on premature mortality in the USA, Air Qual. Atmos. Health, 6, 563–573, doi:10.1007/s11869-013-0197-8, 2013.

Pye, H. O. T., Liao, H., Wu, S., Mickley, L. J., Jacob, D. J., Henze, D. K., and Seinfeld, J. H.: Effect of changes in climate and emissions on future sulfate-nitrate-ammonium aerosol levels in the United States, J. Geophys. Res.-Atmos., 114, D01205, doi:10.1029/2008JD010701, 2009.

Rienecker, M. M., Suarez, M. J., Todling, R., Bacmeister, J., Takacs, L., Liu, H.-C., Gu, W., Sienkiewicz, M., Koster, R. D., Gelaro, R., Stajner, I., and Nielsen, J. E.: The GEOS-5 Data Assimilation System-Documentation of Versions 5.0.1 and 5.1.0, and 5.2.0, NASA Tech. Rep. Series on Global Modeling and Data Assimilation, NASA/TM-2008-104606, vol. 27, Goddard Space Flight Center, Greenbelt, Maryland, USA, 92 p., 2008.

Rind, D., Lerner, J., Jonas, J., and McLinden, C.: Effects of resolution and model physics on tracer transports in the NASA Goddard Institute for Space Studies general circulation models, J. Geophys. Res.-Atmos., 112, D09315, doi:10.1029/2006JD007476, 2007.

Rood, R. B.: Numerical advection algorithms and their role in atmospheric transport and chemistry models, Rev. Geophys., 25, 71–100, doi:10.1029/RG025i001p00071, 1987.

Rotman, D. A., Atherton, C. S., Bergmann, D. J., Cameron-Smith, P. J., Chuang, C. C., Connel, P. S., Dignon, J. E., Franz, A., Grant, K. E., Kinnison, D. E., Molenkamp, C. R., Proctor, D. D., and Tannahill, J. R.: IMPACT, the LLNL 3-D global atmospheric chem-

ical transport model for the combined troposphere and stratosphere: model description and analysis of ozone and other trace gases, J. Geophys. Res.-Atmos., 109, D04303, doi:10.1029/2002JD003155, 2004.

Santillana, M., Zhang, L., and Yantosca, R.: Estimating numerical errors due to operator splitting in global atmospheric chemistry models: transport and chemistry, available at: http://arxiv.org/pdf/1505.02835v1.pdf (last access: 29 October 2015.

Sillman, S., Logan, J. A., and Wofsy, S. C.: A regional scale model for ozone in the United States with subgrid representation of urban and power plant plumes, J. Geophys. Res., 95, 5731–5748, doi:10.1029/JD095iD05p05731, 1990.

Sportisse, B.: An analysis of operator splitting techniques in the stiff case, J. Comput. Phys., 161, 140–168, doi:10.1006/jcph.2000.6495, 2000.

Strang, G.: On the construction and comparison of difference schemes, SIAM J. Numer. Anal., 5, 506–517, doi:10.1137/0705041, 1968.

Thompson, T. M., Saari, R. K., and Selin, N. E.: Air quality resolution for health impact assessment: influence of regional characteristics, Atmos. Chem. Phys., 14, 969–978, doi:10.5194/acp-14-969-2014, 2014.

van Donkelaar, A., Zhang, L., Chen, D., Martin, R. V., Pasch, A. N., Szykman, J. J., and Wang, Y. X.: Improving the accuracy of daily satellite-derived ground-level fine aerosol concentration estimates for North America, Environ. Sci. Technol., 46, 11971–11978, doi:10.1021/es3025319, 2012.

Vinken, G. C. M., Boersma, K. F., Jacob, D. J., and Meijer, E. W.: Accounting for non-linear chemistry of ship plumes in the GEOS-Chem global chemistry transport model, Atmos. Chem. Phys., 11, 11707–11722, doi:10.5194/acp-11-11707-2011, 2011.

Wang, Q., Jacob, D. J., Fisher, J. A., Mao, J., Leibensperger, E. M., Carouge, C. C., Le Sager, P., Kondo, Y., Jimenez, J. L., Cubison, M. J., and Doherty, S. J.: Sources of carbonaceous aerosols and deposited black carbon in the Arctic in winter-spring: implications for radiative forcing, Atmos. Chem. Phys., 11, 12453–12473, doi:10.5194/acp-11-12453-2011, 2011.

Wang, Y., Jacob, D. J., and Logan, J. A.: Global simulation of tropospheric $O_3$-$NO_x$-hydrocarbon chemistry: 1. Model formulation, J. Geophys. Res., 103, 10713–10725, doi:10.1029/98JD00158, 1998.

Wang, Y. X., McElroy, M. B., Jacob, D. J., and Yantosca, R. M.: A nested grid formulation for chemical transport over Asia: applications to CO, J. Geophys. Res., 109, doi:10.1029/2004JD005237, 2004.

Title Page

Abstract | Introduction

Conclusions | References

Tables | Figures

◀◀ | ▶▶

◀ | ▶

Back | Close

Full Screen / Esc

Printer-friendly Version

Interactive Discussion

Wesely, M. L.: Parameterization of surface resistances to gaseous dry deposition in regional-scale numerical models, Atmos. Environ., 23, 1293–1304, doi:10.1016/0004-6981(89)90153-4, 1989.

Wild, O. and Prather, M. J.: Global tropospheric ozone modeling: quantifying errors due to grid resolution, J. Geophys. Res., 111, D11305, doi:10.1029/2005JD006605, 2006.

Wu, S., Mickley, L. J., Jacob, D. J., Logan, J. A., Yantosca, R. M., and Rind, D.: Why are there large differences between models in global budgets of tropospheric ozone?, J. Geophys. Res., 112, D05302, doi:10.1029/2006JD007801, 2007.

Yan, Y.-Y., Lin, J.-T., Kuang, Y., Yang, D., and Zhang, L.: Tropospheric carbon monoxide over the Pacific during HIPPO: two-way coupled simulation of GEOS-Chem and its multiple nested models, Atmos. Chem. Phys., 14, 12649–12663, doi:10.5194/acp-14-12649-2014, 2014.

Zhang, L. M., Gong, S. L., Padro, J., and Barrie, L.: A size-segregated particle dry deposition scheme for an atmospheric aerosol module, Atmos. Environ., 35, 549–560, doi:10.1016/S1352-2310(00)00326-5, 2001.

Zhang, L., Jacob, D. J., Downey, N. V., Wood, D. A., Blewitt, D., Carouge, C. C., van Donkelaar, A., Jones, D. B. A., Murray, L. T., and Wang, Y.: Improved estimate of the policy-relevant background ozone in the United States using the GEOS-Chem global model with $1/2° \times 2/3°$ horizontal resolution over North America, Atmos. Environ., 45, 6769–6776, doi:10.1016/j.atmosenv.2011.07.054, 2011.

**Sensitivity of CTM simulations to the temporal resolution**

S. Philip et al.

Title Page

Abstract | Introduction

Conclusions | References

Tables | Figures

◀ | ▶

◀ | ▶

Back | Close

Full Screen / Esc

Printer-friendly Version

Interactive Discussion

**Table 1.** Mean Error* vs. grid resolution with truth at $2° \times 2.5°$ horizontal resolution.

| Species | Simulation Error ($1 \times 10^{-4}$) | |
|---|---|---|
| | $4° \times 5°$ resolution | $2° \times 2.5°$ resolution |
| Nitrogen oxides | 38.04 | 1.64 |
| Secondary inorganic aerosols | 3.06 | 0.07 |
| Ozone | 6.45 | 0.09 |
| Carbon monoxide | 18.47 | 2.44 |

* Mean taken for timesteps ≤ 30 min.
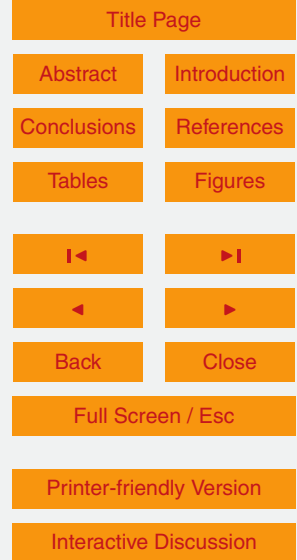
Full Screen / Esc

Printer-friendly Version

Interactive Discussion
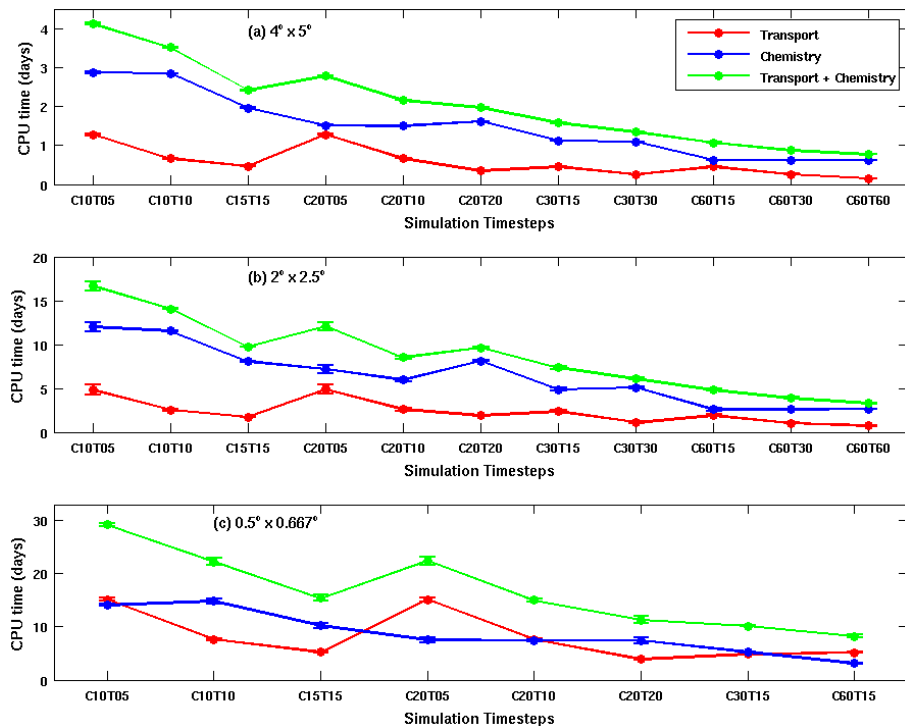


**Figure 1.** CPU time for GEOS-Chem simulations with various timesteps at three horizontal resolutions. Global simulations are at $4° \times 5°$ (top) and $2° \times 2.5°$ (middle) resolutions. The bottom panel contains results for the average of two nested regions North America and East Asia at $0.5° \times 0.667°$ resolution. Colored lines represent the CPU time for simulating transport (red) and chemical (blue) operators, and the sum of the two (green). Error bars represent standard error over five simulations. Simulations are represented in the abscissa as $CccTtt$ with chemical timestep, $C = cc$ min, and transport timestep, $T = tt$ min.
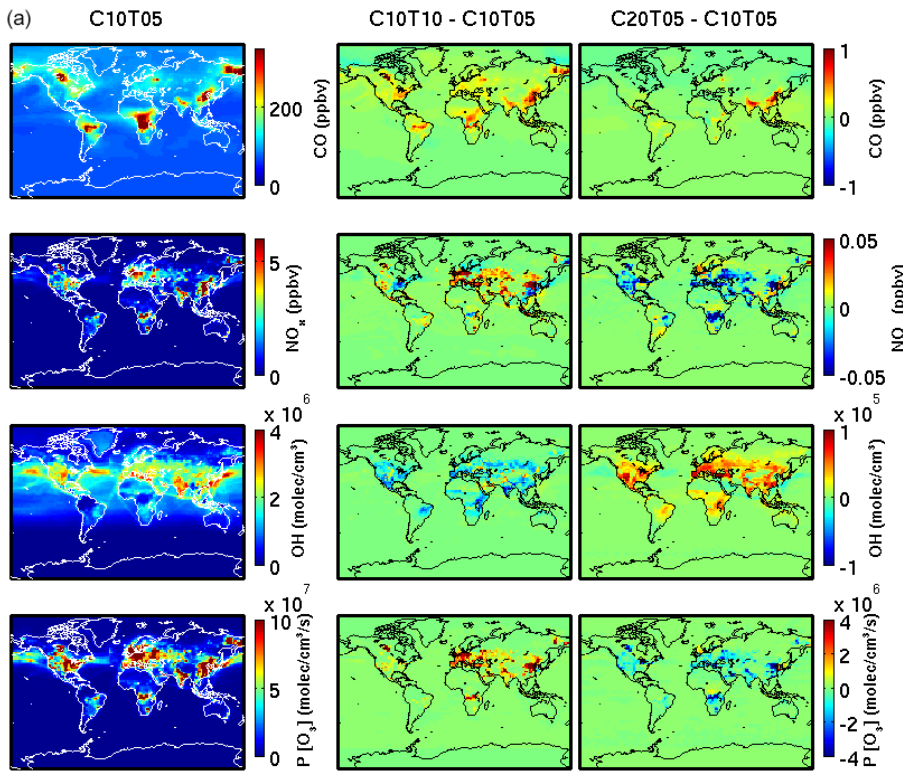
**Figure 2a.** Sensitivity of simulated tracers to the duration of chemical and transport operators. The left column contains monthly mean ground-level concentrations simulated with the finest timesteps considered (C10T05) at $2° \times 2.5°$ horizontal resolution. Other columns contain the absolute differences from doubling the transport timestep to C10T10 (middle), and doubling the chemical timestep to C20T05 (right). Each row from top to bottom represents carbon monoxide (CO), nitrogen oxides (NO$_x$), hydroxyl radical (OH), and the production of ozone (P[O$_3$]). Simulations are represented as $CccTtt$ with chemical timestep, $C = cc$ min, and transport timestep, $T = tt$ min.

Title Page

Abstract | Introduction

Conclusions | References

Tables | Figures

|◀ | ▶|

◀ | ▶

Back | Close

Full Screen / Esc

Printer-friendly Version

Interactive Discussion
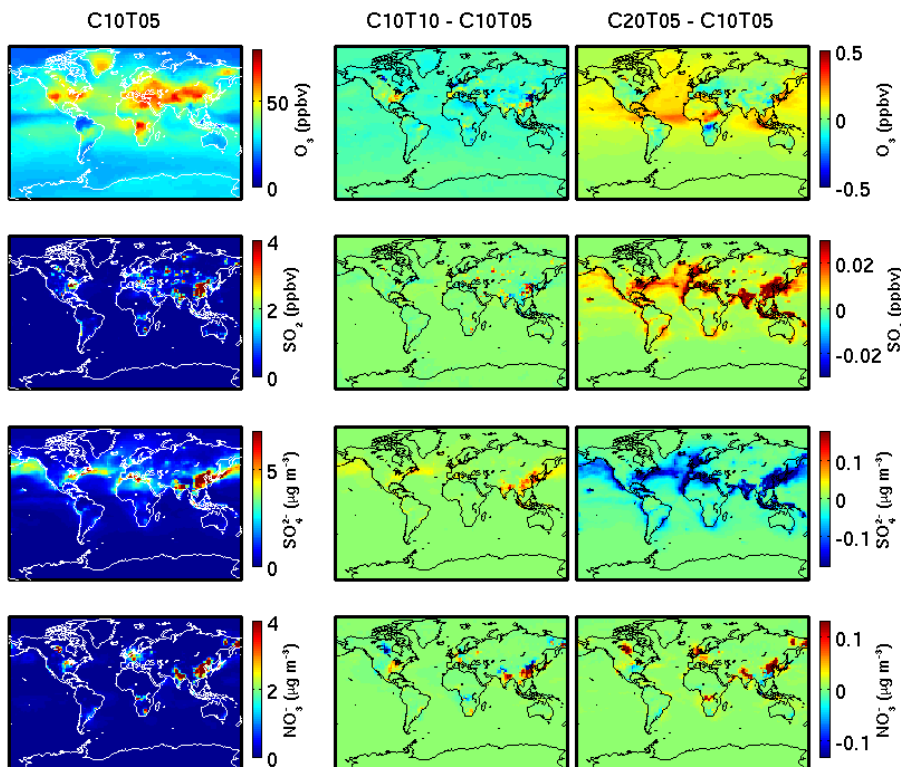
**Figure 2b.** As described in Fig. 2a, but each row from top to bottom represents ozone ($O_3$), sulfur dioxide ($SO_2$), sulfate ($SO_4^{2-}$), and nitrate ($NO_3^-$) respectively.
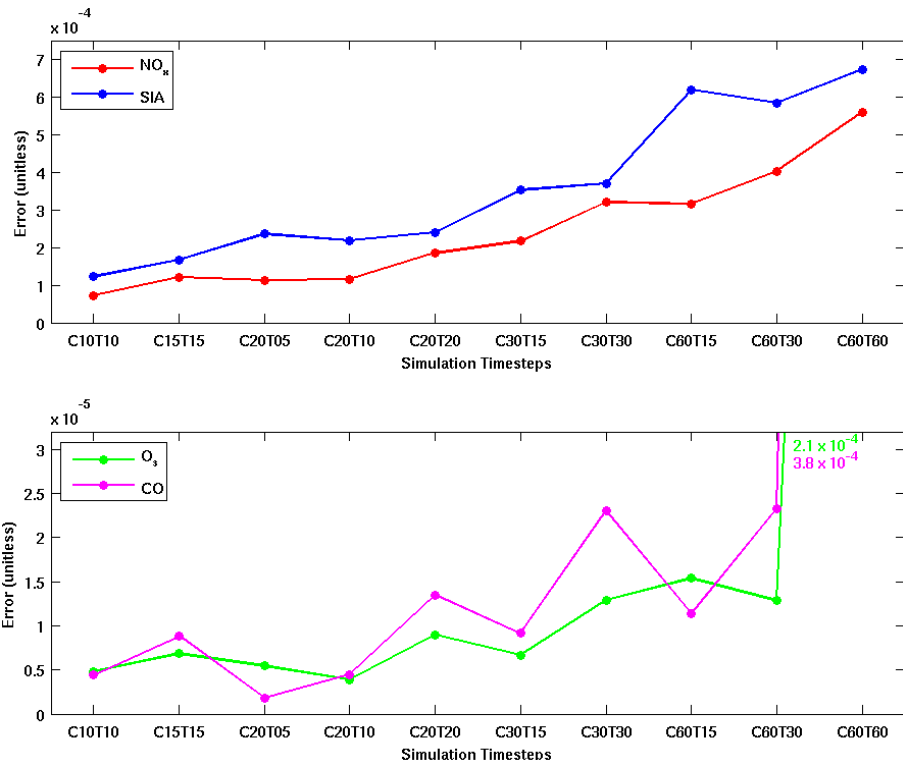
**Figure 3.** Simulation error of different species ($E^s_{sim}$, Eq. 4) for GEOS-Chem with various timesteps at 2° × 2.5° horizontal resolution. Colored lines and dots represent the simulation error for nitrogen oxides (NO$_x$; red), secondary inorganic aerosols (SIA; blue), ozone (O$_3$; green), and carbon monoxide (CO; magenta). Simulations are represented in the abscissa as $CccTtt$ with chemical timestep, $C = cc$ min, and transport timestep, $T = tt$ min.
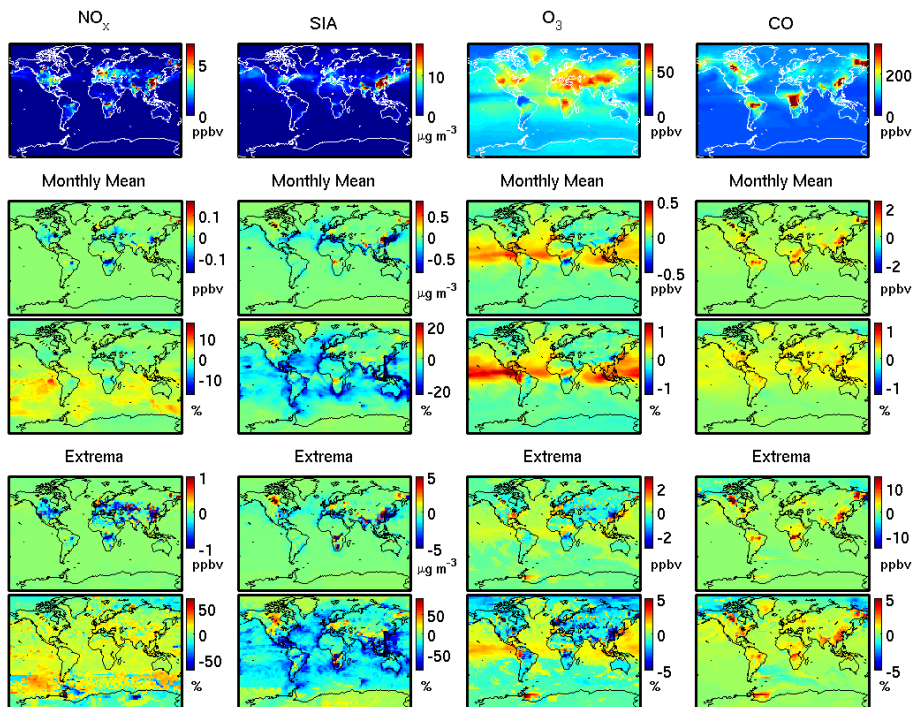
**Figure 4.** Effect on simulated tracers of changing from the GEOS-Chem traditional timesteps (C30T15) to the finest timesteps considered (C10T05). The top row contains ground-level concentrations simulated with the C30T15 timesteps at 2° × 2.5° horizontal resolution. The next two rows contain the monthly mean differences (C30T15 minus C10T05) for absolute (second row) and relative (third row) differences. The two lowest rows contain the maximum differences (C30T15 minus C10T05) for absolute (fourth row) and relative (bottom row) differences. Each column from left to right represents nitrogen oxides (NO$_x$), secondary inorganic aerosols (SIA), ozone (O$_3$), and carbon monoxide (CO).

Title Page

Abstract | Introduction

Conclusions | References

Tables | Figures

|◄ | ►|

◄ | ►

Back | Close

Full Screen / Esc

Printer-friendly Version

Interactive Discussion

**Figure 5.** Normalized error (NE, Eq. 5) for GEOS-Chem simulations with various spatial and temporal resolutions. Colored lines and dots represent the NE for the global simulations at $4° × 5°$ (red) and $2° × 2.5°$ (blue), and the nested simulations at $0.5° × 0.667°$ (green) horizontal resolutions. Error bars represent standard error in CPU time. Simulations are represented in the abscissa as $CccTtt$ with chemical timestep, $C = cc$ min, and transport timestep, $T = tt$ min.

Title Page

Abstract | Introduction

Conclusions | References

Tables | Figures

|◄ | ►|

◄ | ►

Back | Close

Full Screen / Esc

Printer-friendly Version

Interactive Discussion